Effect of Al concentrations on the electrodeposition and properties of transparent Al-doped ZnO thin films

O. Baka, A. Azizi, S. Velumani, G. Schmerber & A. Dinia

Journal of Materials Science: Materials in Electronics

ISSN 0957-4522
Volume 25
Number 4

J Mater Sci: Mater Electron (2014)
25:1761-1769
DOI 10.1007/s10854-014-1796-3

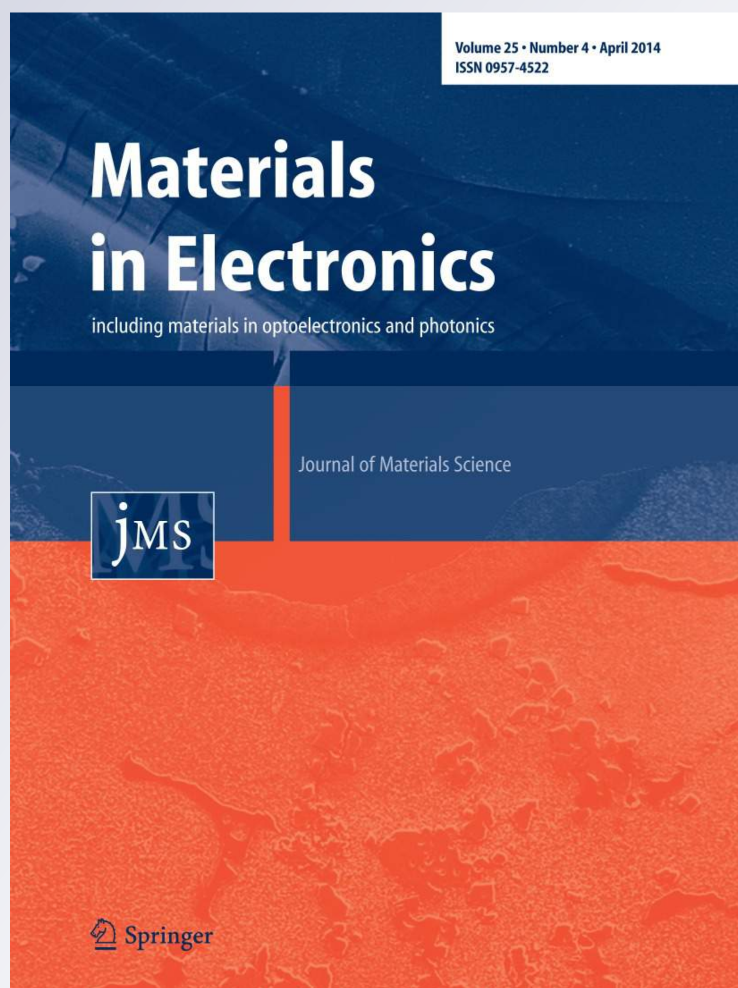

Springer

Your article is protected by copyright and all rights are held exclusively by Springer Science +Business Media New York. This e-offprint is for personal use only and shall not be self-archived in electronic repositories. If you wish to self-archive your article, please use the accepted manuscript version for posting on your own website. You may further deposit the accepted manuscript version in any repository, provided it is only made publicly available 12 months after official publication or later and provided acknowledgement is given to the original source of publication and a link is inserted to the published article on Springer's website. The link must be accompanied by the following text: "The final publication is available at link.springer.com".

Springer

Author's personal copy

J Mater Sci: Mater Electron (2014) 25:1761–1769
DOI 10.1007/s10854-014-1796-3

Effect of Al concentrations on the electrodeposition and properties of transparent Al-doped ZnO thin films

O. Baka · A. Azizi · S. Velumani · G. Schmerber · A. Dinia

Received: 12 December 2013 / Accepted: 10 February 2014 / Published online: 18 February 2014
© Springer Science+Business Media New York 2014

Abstract Al-doped zinc oxide (AZO) thin films are prepared on polycrystalline fluorine-doped tin oxide-coated conducting glass substrates from nitrates baths by the electrodeposition process at 70 °C. The electrochemical, morphological, structural and optical properties of the AZO thin films were investigated in terms of different Al concentration in the starting solution. It was found that the carrier density of AZO thin films varied between −3.11 and $-5.56 \times 10^{20}\ cm^{-3}$ when the Al concentration was between 0 and 5 at.%. Atomic force microscopy images reveal that the concentration of Al has a very significant influence on the surface morphology and roughness of thin AZO. X-ray diffraction spectra demonstrate preferential (002) crystallographic orientation having c-axis perpendicular to the surface of the substrate and average crystallites size of the films was about 33–54 nm. With increasing Al doping, AZO films have a strong improved crystalline quality. As compared to pure ZnO, Al-doped ZnO exhibited lower crystallinity and there is a shift in the (002) diffraction peak to higher angles. Due to the doping of Al of any concentration, the films were found to be showing >80 % transparency. As Al concentration increased the optical band gap was also found to be increase from 3.22 to 3.47 eV. The room-temperature photoluminescence spectra indicated that the introduction of Al can improve the intensity of ultraviolet (UV) emission, thus suggesting its greater prospects in UV optoelectronic devices. A detailed comparison and apprehension of electrochemical, optical and structural properties of ZnO and ZnO:Al thin films is done for the determination of optimum concentration of Al doping.

O. Baka · A. Azizi (✉)
Laboratoire de Chimie, Ingénierie Moléculaire et Nanostructures, Université Ferhat Abbas-Sétif 1, 19000 Sétif, Algeria
e-mail: aziziamor@yahoo.fr

S. Velumani
Centro de Investigacion y de Estudios Avanzados del I.P.N (CINVESTAV), Av. Instituto Politecnico Nacional # 2508, Col. San Pedro Zacatenco, 07360 Mexico, DF, Mexico

G. Schmerber · A. Dinia
Institut de Physique et Chimie des Matériaux de Strasbourg (IPCMS), UMR 7504 CNRS and University of Strasbourg, 23 rue du Loess, B.P. 43, 67034 Strasbourg Cedex 2, France

1 Introduction

As an important low-cost basic II–VI functional semiconductor material, zinc oxide (ZnO) has attracted much interest in both fundamental research and various device applications because of its excellent catalytic, optical, electrical, optoelectronic, gas-sensing, piezoelectric, and photoelectrochemical properties [1, 2]. The incorporation of impurities for altering the properties of ZnO is currently another important issue for possible application in numerous modern technological gadgets. Selective elemental doping in ZnO is proved to be an effective method to tailor with their electrical, optical, and magnetic properties, which is crucial for their practical applications. Therefore, these properties of ZnO thin films can be modified by doping elements such as Al, Ga, Mg, Cd, and Ca [3]. Recently, Al doped ZnO thin films (AZO) have drawn a great deal of attention due to their low material cost, non-toxicity and stability under hydrogen plasma compared to ITO (Sn doped indium oxide) [4]. For example, the incorporation of aluminum could improve the gas-sensor performances of ZnO nanomaterials [5]. In the literature, some research groups have reported that the doping process also affects their properties [6, 7].

Author's personal copy

The most important and intriguing aspect for material scientists is the requirement of an efficient growth technique for ZnO nanostructures with controllable morphology. This needs an emphasis on the comprehension of Al doping on the pattern of its growth along with its influence on the optical properties of ZnO nanostructures.

Al-doped ZnO thin films are prepared by different technologies such as sol–gel, spray pyrolysis, pulsed laser deposition (PLD), magnetron sputtering, and metal organic chemical vapor deposition (MOCVD) [8–12]. Amongst all other methods as mentioned above, electrodeposition technique is intensively employed for production of oxide metallic semiconductor nanostructures with different shape and morphologies [13–16]. It is an established fact that the electrochemical methods offer several advantages including low cost, low operation temperature, large-scale deposition, and ease of mass production [17–19]. Moreover, the preparation of ZnO via electrodeposition is also eco-friendly since there is no usage of toxic chemicals in the electrolytic bath.

Consequently, in this paper, Al-doped ZnO nanostructures were prepared by electrodeposition method from aqueous solution of nitrates of pure Zn and Al salts. The effects of Al doping on the electrochemical, morphologies, microstructures, and optical properties of ZnO nanostructures were studied in detail. The growth mechanism of Al-doped ZnO nanostructures is presumed.

2 Experiment

ZnO thin films were deposited on polycrystalline fluorine-doped tin oxide (FTO)-coated conducting glass substrates by electrodeposition by using hydrate of zinc nitrates as zinc precursor. Analytical grade reagents were used in this electrochemical deposition of ZnO thin films. The $Zn(NO_3)_2$ concentration was kept constant at 0.1 M for all the experiments. Different concentrations of the doping compound $Al(NO_3)_3$ in the electrolyte are explored: 0, 5×10^{-5}, 10^{-4}, 5×10^{-4}, and 5×10^{-3} M $Al(NO_3)_3$; which corresponds to the dopant concentration (Al/Zn at %): 0, 0.05, 0.10, 0.50 and 5.00 at.%, respectively. Therefore, the AZO films with the latter atomic ratio of [Al]/[Zn] were named AZO0, AZO1, AZO2, AZO3 and AZO4, respectively (Table 1). The deposition parameters of the AZO films were kept the same as those for the undoped ZnO film. Deposition temperature was 70 °C. The pH of electrolyte used in this deposition was in the range of 4–6. All samples were controlled to have similar film thickness by the use of same electrical charge. F-doped SnO_2 (FTO, 20–23 Ω sq.$^{-1}$)-coated transparent glasses were used as substrates. Table 1 shows the bath composition and the electro-deposition conditions employed in the preparation of the films. Film thicknesses were measured using a profilometer, KLA Tencor, P15 model. The surface morphology was observed by atomic force microscopy (AFM). The roughness (root-mean-square height deviation) of the samples was obtained directly from the software of the AFM (PicoScan 5.3 from Molecular Imaging). The structure of the films was analyzed by a Rigaku SmartLab diffractometer X-ray diffraction (XRD) diffractometer using Cu Kα_1 radiation at 45 kV and 200 mA (Cu Kα_1, $\lambda = 0.154056$ nm). The electrical properties of AZO films were studied at room temperature using an ECOPIA Hall effect measurement system.

Table 1 Data of the AZO thin films: the $Al(NO_3)_3$ in the electrolyte, the Al concentration in the ZnO thin films, C_{Al} (at.%), the flat band potential and the carrier density (cm^{-3})

Sample	$Al(NO_3)_3$ (M)	C_{Al} (at.%)	E_{fb} (V vs. SCE)	$10^{20} \times N_d$ (cm^{-3})
AZO0	0	0.00	−0.425	-3.11
AZO1	5×10^{-5}	0.05	−0.369	-3.91
AZO2	10^{-4}	0.10	−0.124	-4.17
AZO3	5×10^{-4}	0.50	−0.645	-4.29
AZO4	5×10^{-3}	5.00	−0.956	-5.56

The optical transmittance spectra were obtained with a SHIMADZU 2401PC spectrophotometer in the ultraviolet UV–visible region. The spectra were corrected for glass substrates. Photoluminescence (PL) spectra were conducted at room temperature from the 325 nm line employing a 4 mW He–Cd laser from Kimmon Electric model IK3101R-D.

3 Results and discussions

3.1 Electrochemical study

The electrodeposition process of ZnO is well-known; first, the reduction of nitrate ions produces nitrite and hydroxide ions at the cathode. This was followed by the interaction of Zn with hydroxide ions forming zinc hydroxide. After dehydration of these hydroxides, ZnO is formed as a final product. This mechanism of electrodeposition is simply described as follows [20],

$$Zn(NO_3)_2 \rightarrow Zn^{2+} + 2NO_3^- \quad (1)$$

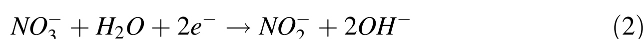

$$NO_3^- + H_2O + 2e^- \rightarrow NO_2^- + 2OH^- \quad (2)$$

$$Zn^{2+} + 2OH^- \rightarrow Zn(OH)_2 \quad (3)$$

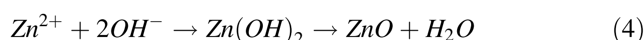

$$Zn^{2+} + 2OH^- \rightarrow Zn(OH)_2 \rightarrow ZnO + H_2O \quad (4)$$

With the presence of Al^{3+} ions in the solution, OH^- ions also react with Al^{3+} ions to form Al_2O_3, which incorporates Al into ZnO and thus dopes the ZnO film:

Author's personal copy

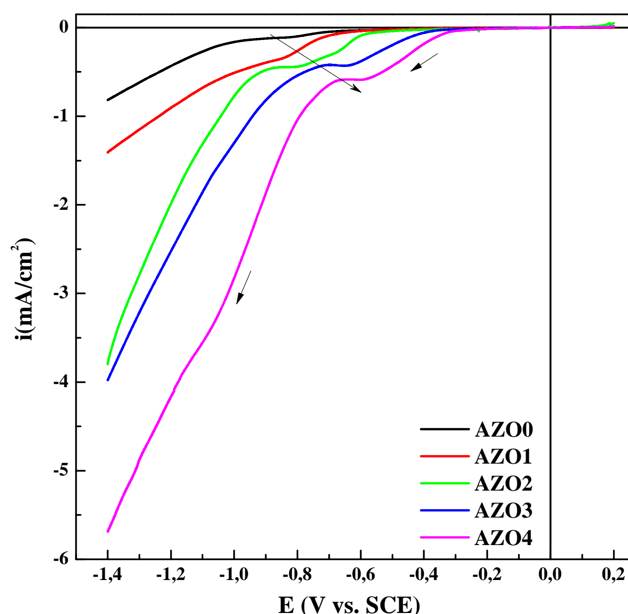

Fig. 1 Cyclic voltammetry (CV) scans of of the electrolytes used for undoped and Al-doped ZnO growth. Only the forward scans (0.2 → −1.4 V) are shown for clarity. The mol% Al in the samples AZO0, AZO1, AZO2, AZO3 and AZO4 are given in Table 1. The scans were performed at a rate of 20 mV/s on FTO substrates

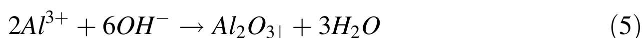

$$2Al^{3+} + 6OH^{-} \rightarrow Al_2O_{3\downarrow} + 3H_2O \quad (5)$$

These reactions may take place in a series or in a parallel/competition way. The deposition product is strongly governed by the deposition conditions, i.e., deposition potential/current, temperature, bath compositions, etc. Practically, the second process is controlled through the deposition potential and the bath concentration, while the third strongly depends on temperature. As for Al doping in ZnO, it is suggested that Al atoms could be incorporated into the lattice of ZnO as substitution for Zn atom sites in previous study. Figure 1 as shown in the cyclic voltammogram was recorded at 70 °C in the potential range from +0.2 to −1.4 V versus SCE in a 0.1 M zinc nitrate solution with different concentrations of $Al(NO_3)_3$ [0–5 mM] at 20 mV s^{-1}. In the latter figure two reduction reactions in this potential range are observed, one reduces nitrate ions to hydroxyl ions ($NO_3^- \rightarrow OH^-$) which corresponds to Eq. 2, occuring around −0.70 V vs. SCE. The other reaction reduces Zn^{2+} ions obtained from Eq. 1 to metallic Zn, which occurs below around −1.0 V. When the applied potential is around −0.75 V, OH^- ions are produced in the deposition solution, which in turn react with Zn^{2+} ions in the solution to form ZnO (Eq.3). It is well observed in this figure that the voltammogram of Al-doped ZnO shifts the electrodepositing potential in the positive region (Fig. 1).

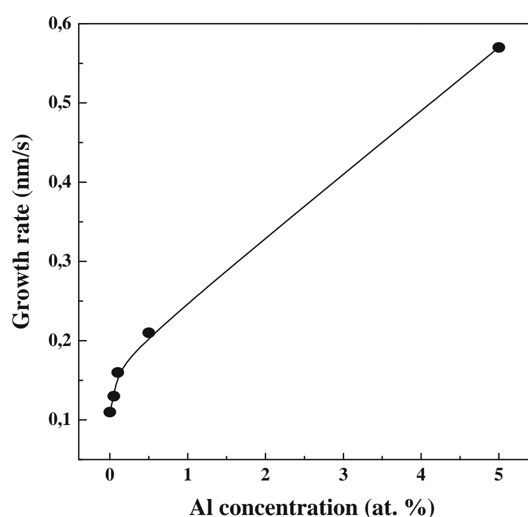

Fig. 2 Growth rate of ZnO nanostructures as a function of Al concentration in the growth solution

On the basis of the cyclic voltammogram curves, it is evident that the presence of Al^{3+} in the growth solution influences the reaction environment and should cause the ZnO nanostructure growth rate to increase. The effects of the Al concentration during growth on the rate of ZnO nanostructures deposition can be seen in Fig. 2. This figure is obtained at a constant deposition temperature (70 °C) and deposition potential (−1.1 V). A distinct increase in the growth rate is observed when Al^{3+} is initially added to the electrolyte, and then for higher Al concentrations, the growth rate slowly continues to increase. The deposition rates ranging from 0.1 to 0.57 nm/s are obtained depending on the Al^{3+} concentration from 0 to 5 mM. This result reveals that the deposition rate of AZO thin films could be controlled by adjusting the Al concentration. The changes in the ZnO growth rate related to the presence of Al^{3+} in the electrolyte correlate well with the CV curve. The growth rate curve indicates that it is possible the deposition process becomes too fast to maintain uniform nanostructures growth at the very large current densities created by high Al concentrations (≥1 % Al). Similar current density increases have been observed in other research on the electrochemical growth of doped ZnO [21, 22].

The Al-ZnO carrier concentration was estimated from Mott–Schottky (MS) measurements. This method is based on the Schottky barrier formation between the semiconductor material and an electrolyte [23–25]. The technique involves measuring the capacitance of the space charge region (C_{sc}) as a function of electrode potential under depletion condition and is based on the MS relation [26]:

$$\frac{1}{C_{sc}^2} = \frac{2}{\varepsilon\varepsilon_0 N_d A^2}\left(E - E_{fb} - \frac{kT}{e_0}\right) \quad (6)$$

Author's personal copy

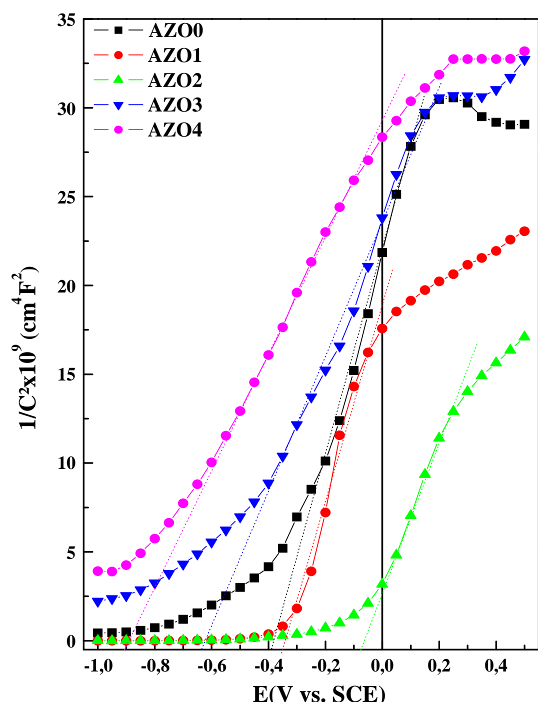

Fig. 3 Mott–Schottky plot for electrodeposited ZnO undoped and doped with Al (AZO) at different concentration. In all cases the employed frequency was 0.2 kHz. The corresponding flat band potential values are indicated. The *lines* were simply drawn through the data points. The plot of ZnO undoped is added for clarity

where ε_0 is the permittivity of free space (8.85×10^{-14} F cm^{-1}), ε is the relative dielectric constant of ZnO (8.5), e_0 is the electron charge, N_d is the free carrier concentration of the semiconductor, A is the area in contact with the electrolyte, E is the applied potential, E_{fb} is the flat band potential, k is the Boltzmann constant (1.38×10^{-23} JK^{-1}), and T is the absolute temperature (298 K). Figure 3 displays the Mott–Schottky curves obtained for the undoped and doped ZnO thin films with Al at different concentrations. All the samples exhibited positive slopes, indicating n-type semiconductor characteristic. It is known from earlier reports that ZnO and Al-doped ZnO films are n-type semiconductors [27, 28]. The slope of tangent line in a Mott–Schottky plot is proportional to $1/N_d$. Table 1 displays the carrier concentration obtained from the linear fitting of the curves. The carrier density fluctuates from -3.11 to -5.56×10^{20} cm^{-3}. This range is in agreement with reported carrier concentrations for Al-doped ZnO [29, 30].

It is shown that carrier concentration of AZO increases with the increase of Al concentration in AZO thin film. The AZO films are n-type semiconductors in nature. The higher donor densities of the samples clearly indicate that there is n doping to the ZnO nanostructures which is in accord with Pradhan et al. [31] measurements. The resources of carrier are due to the doped Al and oxygen vacancies, and the mobility was influenced by a few scattering mechanisms. Also in both figures, the extrapolation of the linear regions in these plots allows us to determine the flat band potential (E_{fb}). The E_{fb} values found at different Al concentration of AZO were shown also in Table 1, which is in agreement with the values reported in the literature [14].

3.2 Morphological analysis

In our experiments, AFM was used to examine the surface morphology of ZnO:Al films. Figure 4 shows AFM images of nanostructured thin films undoped ZnO and doped with Al, deposited at constant charge density. It was found that the films grow with microcrystalline structure. From the images it is seen that all the film surfaces are well covered with the variably distributed spherical grains of varying sizes. It is evidently seen that addition of Al changes the topography of films from clusters into well defined spherical grains. Surface roughness is one of the important properties of the AZO thin films for many opto-electronics applications, because the smooth structure can reduce the scattering of incident light, which makes the contribution to increase the transmittance [32]. Effectively, the surface roughness of the deposited ZnO layers is determined by AFM. Figure 5 shows the root mean square (RMS) roughness of the AZO thin films deposited at constant charge density at various concentrations of Al: 0, 0.05, 0.10, 0.5 and 5.0 at.%. It is found that the surface roughness is strongly dependent on at.% Al. From this figure, when Al concentration increased from 0 to 5 at.%, the RMS roughness increased from 5 to 34 nm. It should noted that the maximum value of RMS was observed at $C_{Al} = 0.5$ and attributed to the rough surface of the AZO film. This phenomenon could affect the band gap energy of the AZO films. After this maximum of RMS, the latter decreased as the aluminum concentrations increased.

3.3 Structural characterization

Figure 6 shows the XRD patterns obtained from undoped and Al-doped ZnO films with different concentrations of $Al(NO_3)_3$ in the electrolyte. All the patterns reveal that the wurtzite structure of ZnO is conserved even after ZnO films are doped with Al. In effect, distinct diffraction peaks, corresponding to the (100), (002), (101), (102), (110), (103), (200) and (112) lattice planes are observed. The intensity of the XRD peaks of ZnO decreases on increasing $Al(NO_3)_3$ concentration in the electrolyte, which demonstrates deterioration of the crystalline structure with Al concentration. The electrodeposited thin films are found to have preferred oriented along (002) plane of the wurtzite structure of ZnO with c-axis normal to the substrate

Author's personal copy

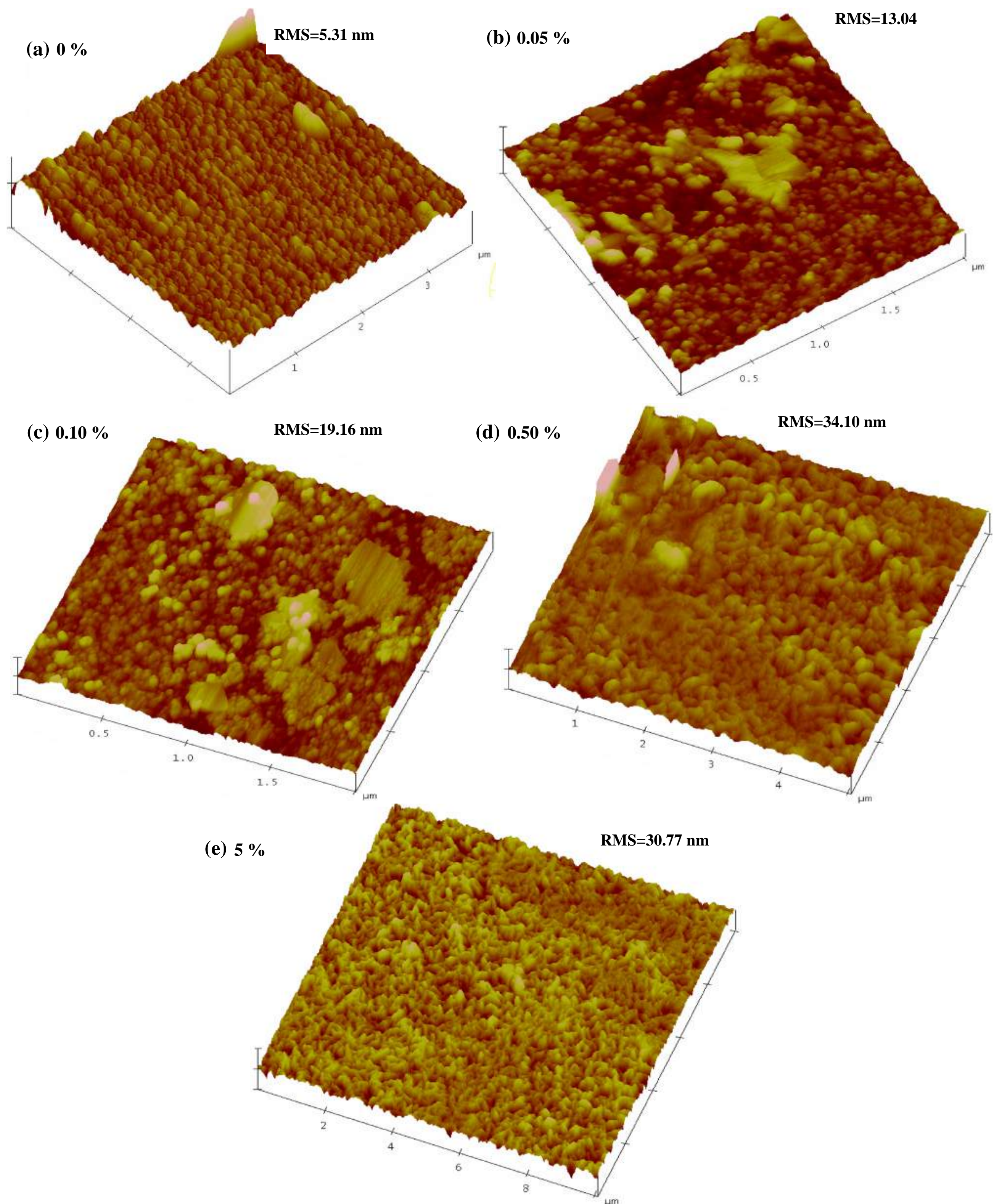

Fig. 4 AFM images of ZnO thin films undoped and doped with Al (AZO) at different concentrations: **a** 0, **b** 0.05, **c** 0.10, **d** 0.50 and **e** 5.00 at.% Al

Author's personal copy

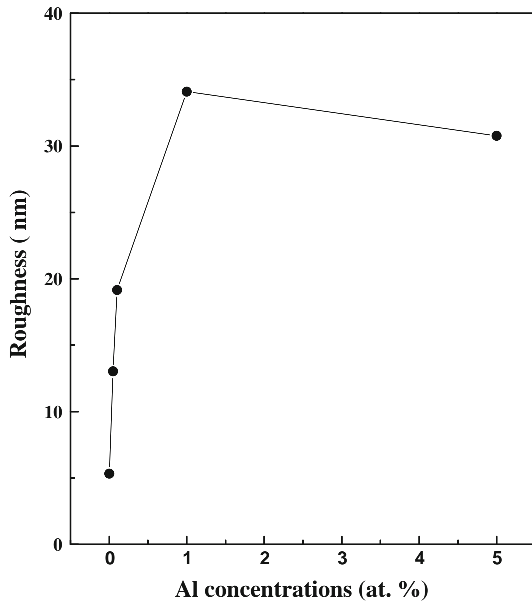

Fig. 5 Variation of the RMS roughness of the AZO thin films with concentrations of Al

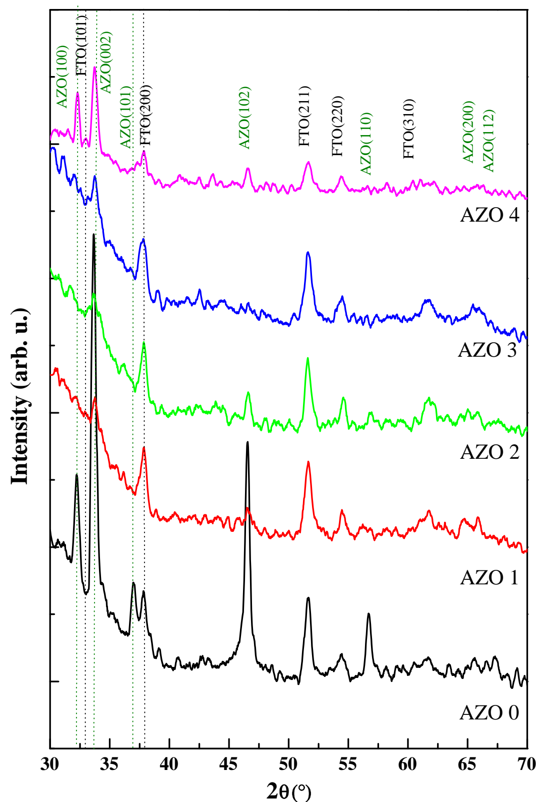

Fig. 6 XRD spectra of the nanostructured thin films of ZnO, undoped and doped with Al. XRD peaks of SnO_2:F (FTO) are marked by *asterisks*. The Al concentration in the samples AZO0, AZO1, AZO2, AZO3 and AZO4 are given in Table 1

Table 2 Displays effect of the Al doping concentration on microstructural and optical properties

Sample	2θ (°)	a (Å)	c (Å)	d (Å)	D (nm)	E_g (eV)
AZO0	33.66	3.258	5.320	2.660	33.66	3.22
AZO1	33.73	3.251	5.310	2.655	43.10	3.41
AZO2	33.67	3.254	5.319	2.659	46.59	3.43
AZO3	33.75	3.249	5.307	2.653	50.63	3.44
AZO4	33.75	3.249	5.307	2.653	54.17	3.47

surface. This preferred orientation is more pronounced at higher concentration of the dopant and intensities of other peaks also increase. It is interesting to note that for all Al doped ZnO thin films, no additional peak corresponding to aluminium or any other phase was observed in the XRD pattern (Fig. 6), indicating the substitution of Al ions at the Zn sites in ZnO lattice. Also, the (002) peak for all the Al:ZnO thin films is obtained at an angle 2θ which is more than the corresponding value reported for bulk ZnO, indicating the presence of dilation stress in all as-deposited Al:ZnO thin films (Table 2). This is probably due to the expansion of the unit cell. This occurs as Al ions with radius 0.51 Å are replaced by Zn ions of larger radius, 0.74 Å. The full-width at half-maximum (FWHM) of the (002) peak are estimated by fitting using X'Pert HighScore software provided by PANalytical. When the Al content in ZnO increases, the FWHM of (002) peak becomes slightly broader indicating that the crystallite size of the Al:ZnO thin films increases with increase in Al content in the films. This result is consistent with other measurements [32, 33].

Assuming a homogeneous strain across crystallites, the average crystallites size can be estimated from the FWHM values of the diffraction peaks. An average size of the crystallites in the direction perpendicular to the plane of the films could be obtained using the Scherrer equation [34]:

$$D = \frac{k\lambda}{\beta \cos\theta} \qquad (7)$$

where D, θ, and λ are the mean crystallites size, the Bragg angle, and the wavelength of the incident X-ray (0.15406 nm), respectively. K is a shape factor and usually takes a value of 0.94.

The calculation of the average size of the crystallites of as-grown undoped and doped ZnO samples electrodeposited at different concentrations of $Al(NO_3)_3$ in the electrolyte estimated from (002) diffraction peak are listed in Table 2. It is known that the term "crystallites size" means the dimensions of the coherent diffracting domain. Therefore, this formula is applicable to thin films where lattice strain is absent. Electrodeposited thin films can possess

Author's personal copy

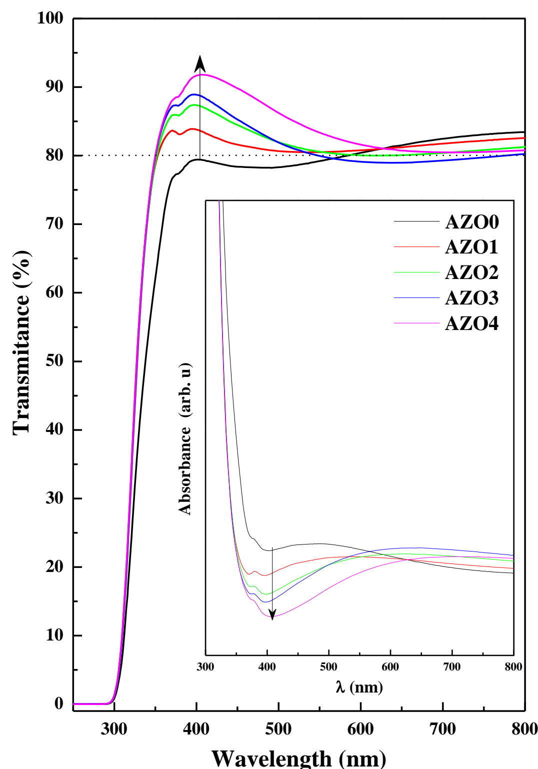

Fig. 7 Transmittance spectra of the ZnO and Al-doped ZnO (AZO) thin films growth on FTO substrates at different Al concentrations, deposited at constant charge density. The *inset* shows the corresponding absorbance spectra

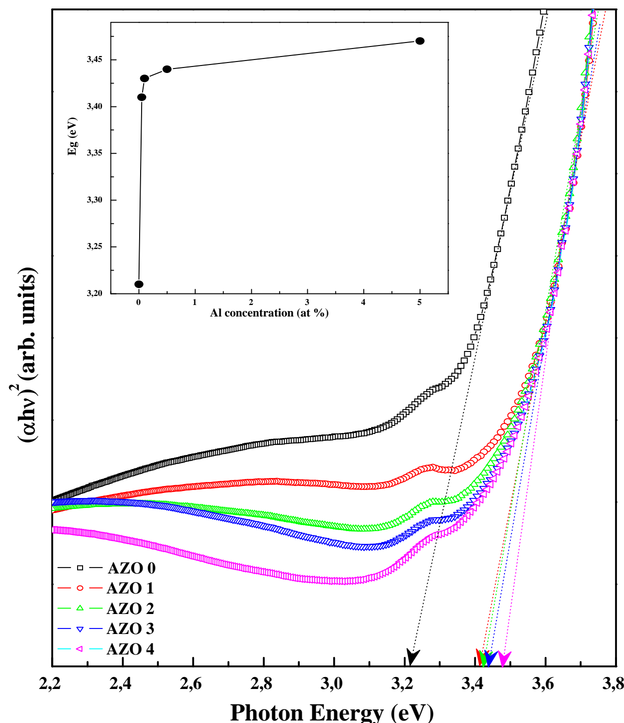

Fig. 8 Plot $(\alpha h\upsilon)^2$ versus hυ for undoped and doped ZnO thin films deposited on conductive FTO electrode. The band gap values obtained by extrapolating the linear part of the curves are also shown

some strains, which could also contribute to peak widening, thereby affecting the estimation of the crystallites size. Therefore, the size of the crystalline domains determined from the XRD peak widths is used only as a comparative parameter among samples [35].

3.4 Optical properties

The transmittance spectra with wavelength from 200 to 800 nm of ZnO pure and AZO thin films at different doping concentrations are shown in Fig. 7. The dotted line which is parallel to X-axis is due to light transmittance of 80 %. It may be seen from this figure that all the prepared ZnO:Al thin films exhibited high optical transmittance (>80 %) in the visible region, and a sharp fundamental absorption edge was observed at around 380 nm. Optical transmission in the visible range is important for TCO applications such as solar cell windows. The high optical transmittance of the investigated AZO film in the visible light region is attributed to the high transmittance near the infrared regions. This observation can be explained by the Burstein-Moss effect in which the lowest states in the conduction band are blocked and only transitions to energies that are above the Fermi level can take place [36, 37].

In order to determine optical band gap of this material and the type of optical absorption, Tauc [38], and Davis and Mott [39] showed that the absorption coefficient and photon energy are related by the following equation:

$$\alpha h\nu = A\left(h\nu - E_g\right)^n \tag{8}$$

In the above equation, A is a constant, E_g is the band gap of the material, and n has different values depending on the optical absorption process. It was found that n = 1/2 which is the best fit for our results and is a characteristic of the direct band gap absorption without phonon mediation. Figure 8 shows the plot of $(\alpha h\nu)^2$versus the photon energy (hν) from which the optical band gap was determined. Accordingly, the optical band gap can be obtained by extrapolating the corresponding straight lines downwards to the photon energy axis in the Tauc plot [38]. In the insert of Fig. 8 is presented the variation of the values of E_g with Al-doping. The optical band gap increased in accordance with an increase in the Al doping concentrations. The value of AZO thin films is about from 3.41 to 3.47 eV.

According to the Burstein-Moss effect [39, 40], the broadening of the optical band gap is given as follows:

$$\Delta E_g = \left(\frac{h^2}{2m^*_{vc}}\right)\left(3\pi^2 n\right)^{\frac{2}{3}} \tag{9}$$

Author's personal copy

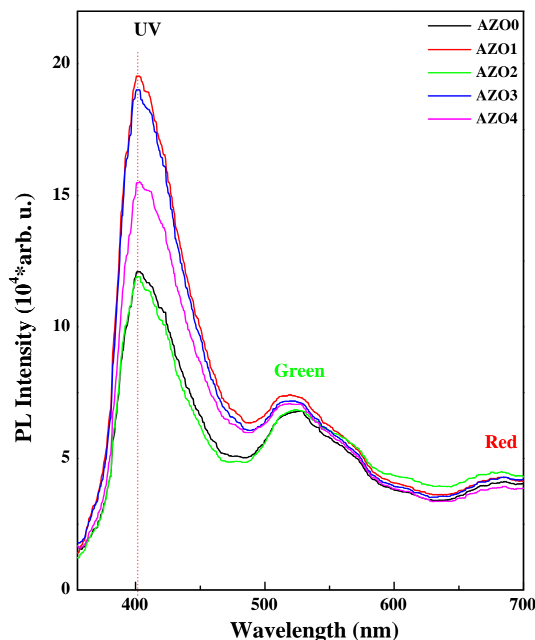

Fig. 9 Room-temperature PL spectra of ZnO thin films undoped and doped with Al at different Al concentrations, deposited at constant charge density

where ΔE_g is the shift of the doped semiconductor compared to undoped semiconductor, m^*_{vc} is the reduced effective mass, h is the Plank constant, and n is the carrier concentration. According to this equation, the optical band gap would increase with increasing carrier concentration.

The optical quality and the possible effects of Al-doping were checked using room temperature PL. It is a well known fact that the PL spectra reveal the presence of impurities and lattice defects that result in the formation of impurity levels in the band gap, which, in turn, decrease the intensity of exciton luminescence bands and give new luminescence bands. Figure 9 shows the room temperature PL spectra of the undoped and doped ZnO at different Al concentrations. As shown in this latter figure, the PL spectra of ZnO and AZO thin films show two distinct peaks: one narrow peak in the UV region and one broad green band centered at about 398 and 500 nm, respectively. The UV emission originates from the recombination of the free excitons of ZnO [41–44] and the defect-related green band is believed to relate to oxygen vacancies. Also, all films exhibited a red emission peak at 680 nm. It can be seen from Fig. 9 that the peak intensity of UV emission varies with Al concentrations. The ZnO nanostructures doped with 1 % Al shows strong UV emission and high intensity ratio of UV to visible emission (I_{UV}/I_{Vis}) as compared to other concentrations of Al. The intensity ratio of UV emission to visible emission (I_{UV}/I_{Vis}) is usually employed as an important criterion to indirectly evaluate the quality of AZO. The UV emission of ZnO doped with Al concentration of 0.05, 0.10, 0.50 and 5 at.% show red shift, which is probably due to the band gap shifting to the lower energy. This reveals that the ZnO nanostructures with Al doping concentration of 1 at.% has strong optical quality than other lower doping concentration.

4 Conclusion

Aluminum doped ZnO nanostructures were synthesized by electrochemical method at various Al concentrations in a nitrates aqueous solution. The voltammogram of Al-doped ZnO shifts the electrodepositing potential in the positive region. From the Mott–Schottky measurements, all AZO thin films presented the carrier density between −3.10 and -5.60×10^{20} cm^{-3} when the Al concentration was varied between 0 and 5 at.%. AFM analysis shows an increase in the roughness with increase of Al concentration in the layer of AZO thin films. XRD measurements reveal that the introduction of Al dopant causes the shift of diffraction peaks and the decrease of crystallinity. Lattice parameters were determined using XRD data and they exhibit wurtzite structure. It is found that the average crystallite size calculated using Scherrer's formula is in the range of 33–54 nm. The optical measurements of all the samples with different aluminum concentrations were found to be >80 % thus demonstrating that all films are highly transparent in nature. The band gaps are found to increase from 3.22 eV for undoped ZnO thin films to 3.47 eV for Al-doped ZnO thin films and it is observed that the band gap increases with the Al concentration in ZnO films. The effect of Al doping on optical properties was also studied by PL spectra, which indicates that the strong UV emission in Al-doped ZnO nanostructures is connected with the FX LO phonon replica emission. The room-temperature PL spectra indicate finally that the introduction of Al can improve the intensity of UV emission, suggesting greater application prospect in UV optoelectronic devices.

Acknowledgments The authors wish to acknowledge the DG-RSDT/MESRS, Algeria, for the financial support through the PNR program (2011–2013).

References

1. K.X. Yao, H.C. Zeng, J. Phys. Chem. B. **110**, 14736–14743 (2006)
2. Z.L. Wang, J.H. Song, Science **312**, 242–246 (2006)
3. A. Stadler, Materials **5**, 661 (2012)
4. E. Fu, D. Zhuang, G. Zhang, Z. Ming, W. Yang, J. Liu, Microelectron. J. **35**, 383–387 (2004)
5. Z.X. Yang, Y. Huang, G.N. Chen, Z.P. Guo, S.Y. Cheng, S.Z. Huang, Sens. Actuators B. Chem. **140**, 549 (2009)
6. X.B. Wang, C. Song, K.W. Geng, F. Zeng, F. Pan, J. Phys. D Appl. Phys. **39**, 4992 (2006)

Author's personal copy

7. Z.F. Liu, F.K. Shan, J.Y. Sohn, S.C. Kim, G.Y. Kim, Y.X. Li, Y.S. Yu, J. Electroceram. **13**, 183 (2004)
8. Z.A. Wang, J.B. Chu, H.B. Zhu, Z. Sun, Y.W. Chen, S.M. Huang, Solid State Electron. **53**, 1149 (2009)
9. J.L. Chen, D. Chen, Z.H. Chen, Mater. Sci. Technol. **26**, 47 (2010)
10. L. Dghoughi, F. Ouachtari, M. Addou, B. Elidrissi, H. Erguig, A. Rmili, A. Bouaoud, Phys. B **405**, 2277 (2010)
11. L. Gong, Z.Z. Ye, J.G. Lu, L.P. Zhu, J.Y. Huang, X.Q. Gu, B.H. Zhao, Vacuum **84**, 947 (2010)
12. M.E. Fragala, G. Malandrino, M.M. Giangregorio, M. Losurdo, G. Bruno, S. Lettieri, L.S. Amato, P. Maddalena, Chem. Vap. Depos. **15**, 327 (2009)
13. C.J. Lan, J.S. Tsay, C.K. Lo, C.A. Lin, J.H. He, R.J. Chung, J. Electrochem. Soc. **157**(11), D559–D563 (2010)
14. M.R. Khelladi, L. Mentar, A. Beniaiche, L. Makhloufi, A. Azizi, J. Mater. Sci.: Mater. Electron. **24**, 153 (2013)
15. M.R. Khelladi, L. Mentar, M. Boubatra, A. Azizi, Mater. Lett. **67**, 331–333 (2012)
16. S. Laidoudi, A.Y. Bioud, A. Azizi, G. Schmerber, J. Bartringer, S. Barre, A. Dinia, Semicond. Sci. Technol. **28**, 115005 (2013)
17. D.Q. Gao, D.S. Xue, Y. Xu, Z.J. Yan, Z.H. Zhang, Electrochim. Acta **54**, 2392 (2009)
18. M.A. Thomas, J.B. Cui, Appl. Phys. Lett. **105**, 093533 (2009)
19. G.R. Li, Q. Bu, F.L. Zheng, C.Y. Su, Y.X. Tong, Cryst. Growth Des. **9**, 1538 (2009)
20. M. Izaki, T. Omi, J. Electrochem. Soc. **143**, L53 (1996)
21. O. Lupan, T. Pauporte, T.L. Bahers, I. Ciofini, B. Viana, J. Phys. Chem. C **115**, 14548 (2011)
22. M. Kemell, F. Dartigues, M. Ritala, M. Leskela, Thin Solid Films **434**, 20 (2003)
23. J. Rousset, E. Saucedo, D. Lincot, Chem. Mater. **21**, 534–540 (2009)
24. C.F. Windisch, G.J. Exarhos, J Vac Sci Technol. **18**, 1677–1680 (2000)
25. I. Mora-Sero′, F. Fabregat-Santiago, B. Denier, J. Bisquert, R. Tena-Zaera, J. Elias et al., Appl. Phys. Lett. **89**, 203117 (2006)
26. S.R. Morrison, *Electrochemistry at semiconductor and oxidized metal electrodes* (Plenum Press, New York, 1980)
27. C.X. Xu, X.W. Sun, X.H. Zhang, L. Ke, S.J. Chua, Nanotechnology **15**, 856 (2004)
28. K.H. Kim, R.A. Wibowo, M. Badrul, Mater. Lett. **60**, 15 (2006)
29. C.H. Huang, H.L. Cheng, W.E. Chang, M.S. Wong, J. Electrochem. Soc. **158**, H510–H515 (2011)
30. H. Wang, M.H. Xu, J.W. Xu, M.F. Ren, L. Yang, J. Mater. Sci.: Mater. Electron. **21**, 589–594 (2010)
31. D. Pradhan, K. Susanta, S. Mohapatra, M. Tymen, K. Misra, T. Leung, Mater. Express **1**, 1 (2011)
32. I.G. Dimitrov, A.O. Dikovska, P.A. Atanasov, T.R. Stoyanchov, T. Vasilev, J. Phys: Conf. Ser. **113**, 012044 (2008)
33. R. Chandramohan, V. Dhanasekaran, S. Ezhilvizhian, T.A. Vijayan, J. Thirumalai, A. John peter, T. Mahalingam, J. Mater. Sci.: Mater. Electron. **23**, 390–397 (2012)
34. R. Jenkins, R.L. Snyder, *Introduction to X-ray powder diffractometry* (Wiley, New York, 1996), p. 89
35. S. Bijani, L. Martínez, M. Gabás, E.A. Dalchiele, J.R. Ramos-Barrado, J. Phys. Chem. C **113**, 19482–19487 (2009)
36. N. Ito, Y. Sato, P.K. Song, A. Kaijio, K. Inoue, Y. Shigesato, Thin Solid Films **496**, 99 (2006)
37. C.G. Jin, T. Yu, Z.F. Wu, F. Wang, M.Z. Wu, Y.Y. Wang, Y.M. Yu, L.J. Zhuge, X.M. Wu, Appl. Phys. A **106**, 961–966 (2012)
38. J. Tauc, in *Optical properties of solids 22*, ed. by F. Abeles (North Holland Pub, Amsterdam, 1970)
39. E. Burstein, Phys. Rev. **93**, 632 (1954)
40. T.S. Moss, Proc. Phys. Soc. Lond. B. **67**, 775 (1954)
41. E.A. Davis, N.F. Mott, Philos. Mag. **22**(179), 903–922 (1970)
42. D. Weissenberger, M. Dürrschnabel, D. Gerthsen, F. Pérez-Willard, A. Reiser, G.M. Prinz, M. Feneberg, K. Thonke, R. Sauer, Appl. Phys. Lett. **91**, 132110 (2007)
43. W.I. Park, Y.H. Jun, S.W. Jung, G–.C. Yi, Appl. Phys. Lett. **82**, 964 (2003)
44. D.C. Reynolds, D.C. Look, B. Jogai, Phys. Rev. B **57**, 12151 (1998)